Critical behavior and transport properties of single crystal $Pr_{1-x}Ca_xMnO_3$ ($x=0.27$, and 0.29)

Wanjun Jiang,* X. Z. Zhou, and Gwyn Williams
Department of Physics and Astronomy, University of Manitoba, Winnipeg, Manitoba, Canada R3T 2N2

Y. Mukovskii and K. Glazyrin
Moscow State Steel and Alloys Institute, Moscow 119049, Russia

(Received 13 June 2008; revised manuscript received 11 September 2008; published 9 October 2008)

A summary of analyses of critical behavior in both the ac susceptibility and dc magnetization in single crystal $Pr_{1-x}Ca_xMnO_3$ ($x=0.27$, and 0.29) is presented supplemented by magnetotransport data. The magnetic data indicate that both single crystals exhibit a continuous/second-order paramagnetic to ferromagnetic phase transition but with marginally different critical exponents. Estimates of the latter for the $x=0.27$ sample yield $\delta=4.81\pm0.02$, $\gamma=1.36\pm0.02$, and $\beta=0.36\pm0.02$ (consistent with both the predictions for the nearest-neighbor three-dimensional-Heisenberg model and with those reported for its double exchange-dominated metallic counterparts) with $T_C=127\pm0.5$ K; whereas at $x=0.29$, $\delta=4.62\pm0.05$, $\gamma=1.38\pm0.01$, and $\beta=0.37\pm0.02$ with $T_C=114\pm0.5$ K. The absence of metallicity—and by inference, the suppression of charge fluctuations—does not, therefore, appear to influence the universality class of the transition. No evidence for a Griffiths-type phase was found in either specimen. These single crystals also display comparable values of the acoustic spin-wave stiffness $D\sim70$ meV Å^2 well below that found in the charge-ordered field-induced metallic regime of the same system. These samples remain insulators below ferromagnetic ordering temperature T_C in fields up to 90 kOe; they display nonabiabatic small polaron mediated transport behavior in the paramagnetic regime in zero field characterized by activation energies comparable to those reported previously for a range of doped perovskites.

DOI: 10.1103/PhysRevB.78.144409 PACS number(s): 75.40.Cx, 75.47.Lx

I. INTRODUCTION

Explanations of the wide-ranging behavior of transition-metal oxides—encompassing high-T_C superconductivity,[1] colossal magnetoresistance (CMR) (Refs. 2–5), and, more recently, multiferroic response[6,7]—continue to present fundamental challenges. In Mn^{3+}/Mn^{4+} mixed-valent manganites in particular, the coupling between charge, spin, orbital, and lattice degrees of freedom is not only in competition but is also characterized by energy scales of comparable magnitude resulting in nearly degenerate ground states displaying marked different ordered features—orbital, magnetic, dielectric, etc.—whose emergence can be controlled by doping, temperature, and other external stimuli. These mixed-valent manganites are characterized by a general formula $(A^{3+})_{1-x}(B^{2+})_x(Mn^{4+})_{1-x}(Mn^{3+})_x(O^{2-})_3$: A being a trivalent rare-earth ion (i.e., Pr, La, Nd, and so on) and B a divalent alkaline-earth cation (i.e., Ca, Ba, Sr, and so on) with x representing the doping level. Changes in x modulate the valence state of the Mn ions to maintain charge neutrality. The accompanying mismatch in the ionic size of ions occupying the "A" site leads to a distortion in the crystal structure frequently characterized by the Goldschmitt "tolerance factor" t_f.[2–5,8] With different doping levels and varying ionic substitutions, the crystal structure transforms from being initially nearly cubic perovskite ($t_f\approx1$) through rhombohedral ($0.96<t_f<1$) and then to an orthorhombic ($t_f<0.96$) structure;[2–5,8] this is accompanied by reductions in the Mn-O-Mn bond angle below the "ideal" 180°, thus reducing the charge-transfer integral and correspondingly the charge mobility.[2–5,8]

In $Pr_{1-x}Ca_xMnO_3$ compound, while complications result for the presence of a Pr moment, this mismatch in the cationic size is minimized generating a pronounced orthorhombic distortion which favors the occurrence of charge localization; $Pr_{1-x}Ca_xMnO_3$, unlike many of its counterparts doped with nonmagnetic rare-earth ions, thus exhibits insulating behavior over an extended temperature range and all doping level in zero field.[2–5,9–14] Nevertheless, in all such materials, disorder plays a pivotal role reflecting the occurrence of nearly degenerate (and hence competing) ground states of very different character. In particular, disorder drives first-order/discontinuous transitions toward second-order/continuous in these systems; $Pr_{1-x}Ca_xMnO_3$, as discussed below, exhibits both types of transition with changing compositions x and disorder underlies spontaneous electronic phase separation (PS): a central component in some theories of CMR.[3,4] Given the insulating ground-state characteristics of $Pr_{1-x}Ca_xMnO_3$, PS scenarios are most frequently discussed in this system in relation to the metal-insulator phase transition accompanying the onset of a charge-ordered state specifically in the higher hole doping range $x\geq0.3$.[3,4,9–14] The simplest representation of PS envisages "domains" with antiferromagnetic (AFM) or insulating and ferromagnetic (FM) or metallic characteristics with the latter being enhanced by applied fields (the conjugate field for ferromagnetism); hence CMR. As a corollary, the exchange bond distribution describing the (magnetic) coupling between spins contains contributions of either sign; however, even when PS does not predominate, the presence of FM Mn^{3+}-Mn^{4+} double exchange (DE) (Ref. 2) and AFM Mn^{3+}/Mn^{4+}-O-Mn^{3+}/Mn^{4+} superexchange (SE) (Ref. 15) results in a comparable exchange bond distribution. If this (assumed Gaussian) distribution is treated in mean field,[16] ferromagnetism emerges when the ratio of the first to second moment of the distribution >1 (i.e., the ratio of the mean

value to the width); however, the precise value for this ratio determines the extent of the FM asymptotic critical regime:[17] a point returned later. The onset of charge order would also play a role in this context. As the relevant interactions in this system are short range, charge ordering would likely result in more bimodal—rather than Gaussian—exchange bond distribution between Mn spins. As bimodal distributions have been investigated far less extensively than their Gaussian counterparts,[18] the composition of the present samples was chosen [guided by the boundaries delineated most recently by the electric-field-gradient (EFG) measurements of Lopes *et al.*[19]] to specifically avoid possible complications arising from charge ordering; this compositional choice was confirmed by measurements of the acoustic spin-wave stiffness discussed later.

$Pr_{1-x}Ca_xMnO_3$ is also unusual in that the application of magnetic fields,[9,10] x-ray irradiation,[11] high electric field,[12] or laser radiation[14] have reportedly induced "unconventional" responses making this system one of the more interesting perovskite manganites.

While at $x=0.3$ the observation of marked hysteresis in both the magnetization $M(T,H)$ and the magnetoresistance $\rho(T,H)$ has led to the associated phase transitions being classified as first order reflecting the importance of AFM interactions,[9,10] for $x<0.3$ FM coupling dominates; nevertheless insulating behavior persists even in high magnetic fields. Previous studies of magnetization and ac susceptibility in this doping range were aimed primarily at establishing the relation between ordering or Curie temperatures and doping levels,[14,20] thus the universality group describing such ordering—best found from single-crystals samples—has not been widely studied. The focus of this paper is to address this deficiency and attempt to resolve the interesting question of whether the lack of metallicity in this system influences magnetic critical behavior. Specifically, in the conventional DE picture, the onset of metallicity is linked with the establishment of an infinite (percolating) pathway of DE metallic bonds—the same bonds that establish an infinite FM "backbone"—so that the emergence of metallicity and ferromagnetism are essentially coincident. This is clearly not the situation encountered in Pr-doped systems; indeed, the insulating ground-state characteristics of the specimens investigated means that any influences of dynamic Mn^{3+}/Mn^{4+} charge fluctuation are curtailed in them.

II. EXPERIMENTAL DETAILS

The two $Pr_{1-x}Ca_xMnO_3$ single crystals used in the present study, with nominal composition $x=0.27$ and 0.29, were grown using a floating zone technique.[21] They were of high structural quality displaying a mosaicity of less than 1°. A Quantum Design model 6000 physical property measurement system (PPMS) magnetometer or susceptometer was used to measure the ac susceptibility $\chi(H,T)$ (at 1 kHz with a 1 Oe rms driving field) and the magnetization $M(H,T)$ at various temperatures T and fields H; the latter being applied along the largest of the approximately $(4\times1\times1)$ mm^3 sample dimensions to minimize demagnetization effects. Prior to measuring at any given temperature, the sample was demagnetized by warming to 300 K—well above the ordering temperature—and then cooling to a predetermined measuring temperature in zero field. The demagnetization factors (N_D) were calculated initially by treating the specimens as an ellipsoids with principal axes equal to the sample dimensions and evaluating the corresponding elliptic integrals yielding $N_D=46\pm1$ g Oe/emu for $x=0.27$ and $N_D=35\pm1$ g Oe/emu for $x=0.29$ (based on the theoretical densities). Magnetoresistance data were acquired with a model 7000 AC transport controller utilizing a conventional four-probe technique with an excitation current of 0.01 mA at 499 Hz supplemented by dc resistivity measurements between 77 and 280 K using a Keithley 224 programmable constant current source and a Keithley 182 digital voltmeter. Contacts to samples with typical dimensions given above were made by compressing indium "pads" over gold current/voltage wires embedded in grooves ground in the samples with a diamond wire saw.

III. RESULTS AND DISCUSSIONS

A. dc magnetization—general features

Figure 1(a) reproduces a series of magnetic isotherms typical of both samples measured here in the vicinity of the ordering temperature (127 K) of the $x=0.27$ sample and at 10 K, the latter typifying those in the liquid-helium range; here the $x=0.27$ specimen displays a small hysteresis ($H_C=228$ Oe) (evident in the insert in this figure) increasing slightly ($H_C=260$ Oe) at $x=0.29$. The response summarized in this figure indicates the absence of a first-order transition at these compositions: an assertion confirmed by the positive slope of all Arrott plots (M/H_i vs H_i^2) isotherms[22,23] shown in Fig. 1(b). Nevertheless the coercive field H_C found in this system far exceeds that reported in single crystals of both its Ca ($x=0.27$, $H_C=4$ Oe) (Ref. 24) and Ba ($x=0.27$, $H_C=6$ Oe) (Ref. 25) counterparts at comparable doping levels: a result likely linked to the presence of moments at the Pr sites.

At $x=0.27$, the saturation magnetization $M_{sat}(T=10\ K)=102.3\pm0.2$ emu/g$=3.97\pm0.03$ μ_B/Mn estimated by extrapolation of M vs H_i^{-1} plot(s) (for 50 kOe$<H<$90 kOe) is some 6% larger than the spin-only Mn^{3+}/Mn^{4+} moment of 3.73 μ_B calculated using the nominal composition indicating a contribution from Pr^{3+} ions of at least ≈0.25 μ_B (a result consistent with that found from neutron-scattering measurements on a $Pr_{0.75}Ca_{0.25}MnO_3$ single crystal[14]). By contrast that found at $x=0.29$ [$M_{sat}(T=10\ K)=96.5\pm0.2$ emu/g $=3.71\pm0.03$ μ_B] is close to the calculated for a spin-only Mn moment (3.71 μ_B) consistent with the absence of a contribution from Pr^{3+} ions. The latter reflects the trend of a decreasing extrapolated moment with increasing x, a trend much more marked above $x=0.3$,[9,10] likely reflecting an increasingly important role played by AFM coupling;[9,10,20] a point returned to below.

Figures 1(c) and 1(d) [($x=0.27$) and ($x=0.29$)] reproduce the temperature dependence of the magnetization measured on warming following zero-field cooling (ZFC) and field cooling (FC) in $H=1$ kOe; these data exhibit a history dependence with a bifurcation between ZFC and FC branches

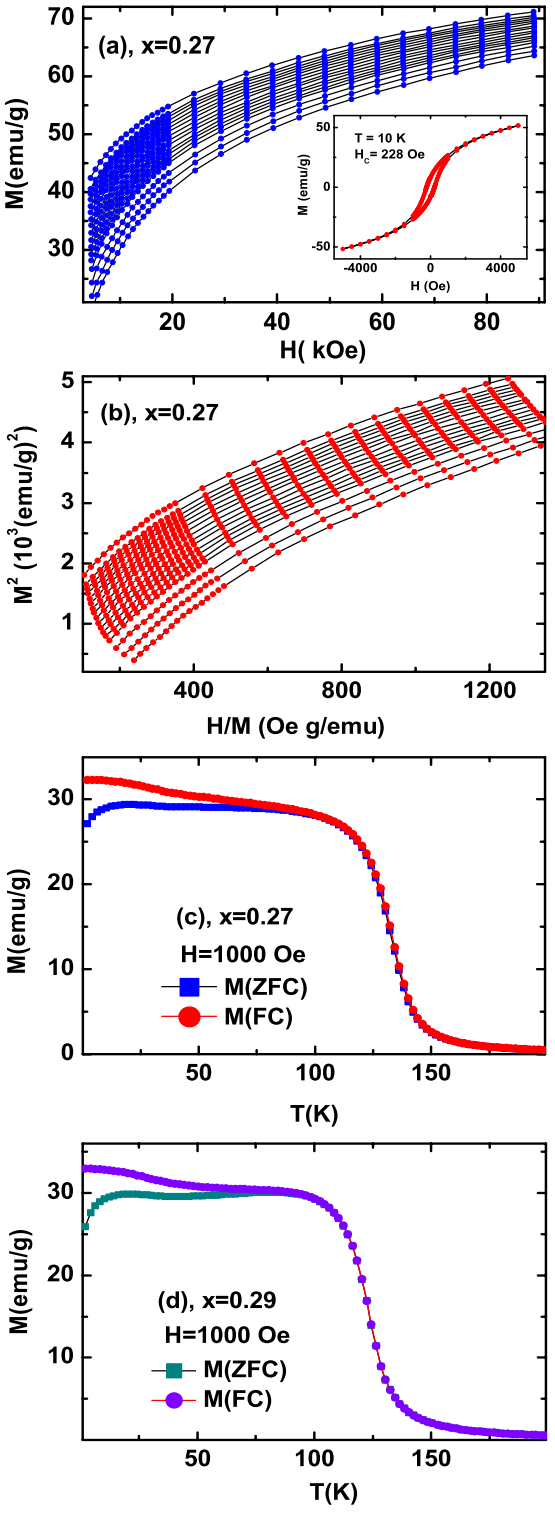

FIG. 1. (Color online) (a) A series of magnetic isotherms collected in increasing field at 120 K, 122 to 134 K in 1 K steps, and 136 to 140 K in 2 K steps: inset; hysteresis loop measurements at 10 K (-5 kOe$<H<5$ kOe) yielding H_C=228 Oe. (b) Arrott plots—H_i/M vs M^2—of the data in (a). (c) Magnetization (measured on warming) vs temperature following ZFC and FC at H =1 kOe for x=0.27. (d) as in (c) for x=0.29.

at $T_{\mathrm{irr}} \approx 126$ and 117 K, respectively,[26] indicating the onset of irreversibility below the ordering temperature. The generic

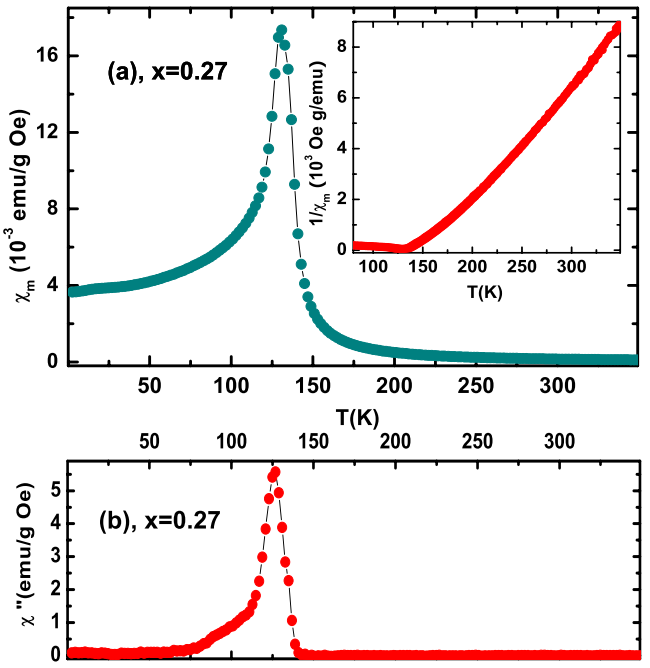

FIG. 2. (Color online) (a) The in-phase zero-field ac susceptibility for x=0.27 measured on warming following ZFC; the Hopkinson/principal maximum is evident at 128 K. Inset: the inverse ac susceptibility displaying no characteristic Griffiths-type phase downturn. (b) The imaginary component of ac susceptibility.

explanation for such behavior is that it reflects the presence of a corrugated free-energy landscape,[27] which—in the specific case of the manganites—likely originates from their intrinsic inhomogeneity, viz., their inhomogeneous mixed-valent Mn^{3+}/Mn^{4+} structures, enhanced here by the rapid increase of AFM interactions as x approaches 0.3.[9,10] In this context it is important to recall that such bifurcation reflects nothing more than the emergence of dissipative processes and, recent simulations show, is suppressed by the application of fields in excess of the coercive field;[27] links between the occurrence of such bifurcation and the onset of PS can thus only be made currently using qualitative arguments especially given the paucity of data exhibiting bifurcation in CMR $La_{1-x}Ca_xMnO_3$ and $La_{1-x}Ba_xMnO_3$ systems in which—in some models of CMR—PS should be prevalent.

B. ac susceptibility—critical behavior

As Fig. 1(b) demonstrates, mean-field exponents fail to linearize Arrott plots near T_C and thus do not provide an appropriate description of the paramagnetic-ferromagnetic (PM-FM) transition in these systems. Figure 2 reproduces the zero-field ac susceptibility for the x=0.27 doped specimen [Figs. 2(a) and 2(b)] being the real and imaginary components, respectively. These data again typify both samples and enable two initial estimates to be made. First, the maximum susceptibility occurring at T=128 K (x=0.27) (at T =116 K at x=0.29) often referred as the Hopkinson/principal maximum[28–32] provides an experimental estimate for the demagnetization factor of $N_D = 1/\chi_{\max}$ =52.2 g Oe/emu (x=0.27) ($N_D = 1/\chi_{\max} = 1/0.02774$

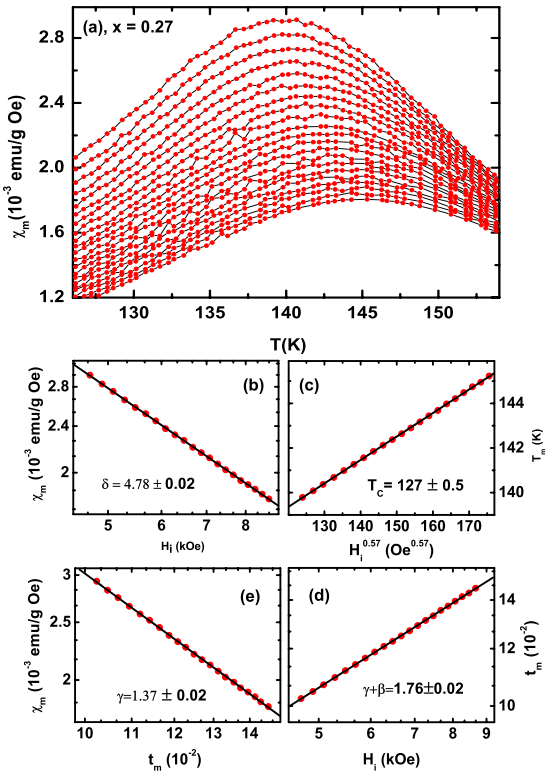

FIG. 3. (Color online) (a) $\chi(H,T)$ for $x=0.27$ (corrected for background and demagnetizing effects) measured on warming following ZFC in fixed static fields of 5 kOe (top) to 9 kOe (bottom) in 200 Oe steps. (b) Double-logarithmic plot testing the power-law prediction of Eq. (3), viz., $\log(\chi_m)$ vs $\log(H_i)$, the slope yielding $\delta=4.78\pm0.02$. (c) Estimate of critical temperature $T_C=127\pm0.5$ K from extrapolation of the susceptibility peak temperatures (T_m) against ($H_i^{0.57}$). Double-logarithmic plots testing the remaining power-law predictions [Eqs. (4) and (5)]. (d) The reduced peak temperature (t_m) against the internal field (H_i), viz., $\log(t_m)$ vs $\log(H_i)$, yielding $\gamma+\beta=1.76\pm0.02$. (e) The peak susceptibilities (χ_m) against reduced temperature (t_m), viz., $\log(\chi_m)$ vs $\log(t_m)$, yielding $\gamma=1.37\pm0.02$ and hence $\beta=0.37\pm0.02$.

$=36.2$ g Oe/emu at $x=0.29$) (values unexpectedly close to theoretical estimates given the nonellipsoidal sample shape) and used subsequently to make demagnetization corrections. Second, the inflection point in ac susceptibility yields preliminary estimates of ordering temperatures, viz., $T_C=125$ K at $x=0.27$, and 117 K at $x=0.29$. The imaginary component at $x=0.27$ [Fig. 2(b)] peaks at $T=127$ K (at 119 K at $x=0.29$) close to T_C and the Hopkinson/principal maximum confirming the onset of irreversible magnetization processes in the ordered phase.

The temperature dependence of the ac susceptibility measured in various superimposed static biasing fields is shown in Fig. 3(a) for the $x=0.27$ sample; data again typical of both specimens. With the applied-field-induced suppression of the Hopkinson maximum, the latter displays a series of peaks which increase in temperature but decrease in amplitude as the static applied field is increased: an unequivocal signature of a continuous/second-order transition.[28,29,31–34] Standard scaling theory predicts that the locus and amplitude of these peaks are governed by a set of power-laws predictions[28,29,31–33] as the following demonstrates with the reduced magnetization written in the usual form, viz.,

$$m(h,t)=|t|^{\beta}F_{\pm}\left(\frac{h}{|t|^{\gamma+\beta}}\right), \tag{1}$$

where $t=(T-T_C)/T_C$ and $h\sim H_i/T_C$ (where the internal field $H_i=H_a-N_DM$, in the usual notation), the susceptibility becomes—assuming the validity of the Widom equality—$\gamma+\beta=\beta\delta$,[34]

$$\chi(h,t)=\frac{\partial m}{\partial h}=|t|^{-\gamma}\cdot G_{\pm}\left(\frac{h}{|t|^{\gamma+\beta}}\right)=h^{1-1/\delta}\cdot H_{\pm}\left(\frac{h}{|t|^{\gamma+\beta}}\right), \tag{2}$$

$G_{\pm}(x)$ being the derivative of the (unknown) scaling function $F_{\pm}(x)$ with respect to its argument. Three power-law dependences follow directly from this equation,[28,29,31–33] viz., for the critical peak amplitude on field [Eq. (3)], for the (reduced) peak temperature on field [Eq. (4)], and for the peak amplitude on (reduced) temperature [Eq. (5)],

$$\chi(H_i,t_m)\propto H_i^{1/\delta-1} \tag{3}$$

$$t_m=(T_m-T_C)/T_C\propto H_i^{1/(\gamma+\beta)} \tag{4}$$

$$\chi_m\propto t_m^{-\gamma}. \tag{5}$$

Here the reduced peak temperature $t_m=(T_m-T_C)/T_C$ determines the location of the "crossover" line—the locus of the susceptibility maxima—above which the response is thermally dominated as opposed to being field dominated below it.[28–33]

The evolution with applied field and temperature of the peak structure evident in Fig. 3(a) provides confirmatory evidence of the continuous nature of the accompanying phase transition supporting the conclusion drawn from Arrott plots. However, the detailed analysis of this peak structure in terms of scaling law predictions reveals slight differences at two doping levels.

$x=0.27$

Figures 3(b)–3(e) summarize the analysis of these ac susceptibility data for $x=0.27$ in terms of scaling law predictions [Eqs. (3)–(5)]. Figure 3(b) reproduces the corresponding critical peak amplitude (corrected for background and demagnetizing effects) against the internal field on a double-logarithmic scale confirming the power-law dependence of Eq. (3) with the slope of this plot yielding $\delta=4.78\pm0.02$ (an estimate clearly independent of any choice for T_C). The latter represents a distinct advantage over conventional magnetization-based approaches for which the determination of the ordering temperature is a prerequisite prior to extracting estimates for δ from data taken along the critical isotherm. Tests of the remaining power laws, however, require an estimate for T_C; this is done initially as shown in Fig. 3(c), viz., by plotting the measured peak temperatures T_m against the internal field $H_i^{0.57}$ [i.e., assuming and following the estimate for δ, the applicability of Heisenberg model exponents, viz. $(\gamma+\beta)^{-1}=0.57$ (Ref. 35)], and extrapolating to

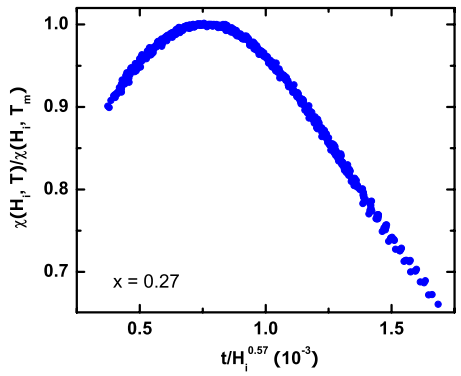

FIG. 4. (Color online) Scaling plot for the isokaps in Fig. 3(a) for $x=0.27$.

$H_i=0$ yielding $T_C=127\pm0.5$ K. This estimate is then used to construct the double-logarithmic plots shown in Figs. 3(d) and 3(e), i.e., of the reduced temperature t_m against the internal field [Eq. (4)] and of the peak amplitude against the reduced temperature t_m [Eq. (5)]. Typically, small adjustments to T_C are then made until a consistent set of plots are established; this proved unnecessary in the present case, with the slopes of the latter two figures yielding $\beta=0.36\pm0.03$ and $\gamma=1.37\pm0.02$ with the same T_C.

A final test of the applicability of three-dimensional (3D)-Heisenberg model exponents[35] to this system is provided in Fig. 4 using ac susceptibility data from Fig. 3(a). Scaling theory in the form summarized in Eq. (2) predicts that such data, when normalized to its peak value $[\chi(h,T_m)]$, should fall on a universal curve when plotted against the argument $(h/t^{(\gamma+\beta)})$ of the scaling function (actually, its inverse $t/h^{1/(\gamma+\beta)}$, which maintains the peak structure[29,36]). In combination, the above shows that these estimates for δ, γ, and β agree, within experimental uncertainty, with 3D-Heisenberg model predictions [$\gamma=1.387$, $\beta=0.365$, and $\delta=4.783$ (Ref. 35)] and satisfy the Widom equality $\gamma=\beta(\delta-1)$.[34]

C. dc magnetization—critical behavior

For the continuous PM-FM transition, the scaling law equation of state [Eq. (1)] leads to the following well-established power-law predictions for the (reduced) spontaneous magnetization $M_S(T)=M_S(H=0,T)$,[28–31,34,37,38]

$$M_S(T) = M_S(0)\left(1-\frac{T}{T_C}\right)^{\beta}; \quad m(0,t)\sim B|t|^{\beta}(T<T_C), \tag{6}$$

the initial susceptibility $[\chi_i(T)=(\partial M/\partial H)_{H=0}]$

$$\chi_i(T) = \chi_0\left(\frac{T}{T_C}-1\right)^{-\gamma}; \quad \chi_i(t)=\frac{\partial m}{\partial h}\sim Ct^{-\gamma}(T>T_C). \tag{7}$$

While along the critical isotherm ($T=T_C$ and $t=0$),

$$M(H,T=T_C)=M_0H^{1/\delta}; \quad m(h,0)\sim Eh^{1/\delta}. \tag{8}$$

These equations form the basis of independent estimates for ordering temperature T_C and the critical exponents γ, β, and δ through the detailed self-consistent analysis of magnetic isotherms.[30,32] Based on an Arrott-Noakes equation of state,[22,23] these data were replotted in the form $(H_i/M)^{1/1.387}$ versus $M^{1/0.365}$ shown in Fig. 5(a). The latter yields a series of parallel straight lines confirming the applicability of 3D-Heisenberg model exponents and an estimated ordering temperature of $T_C=127\pm0.5$ K from the isotherm passing through the origin.

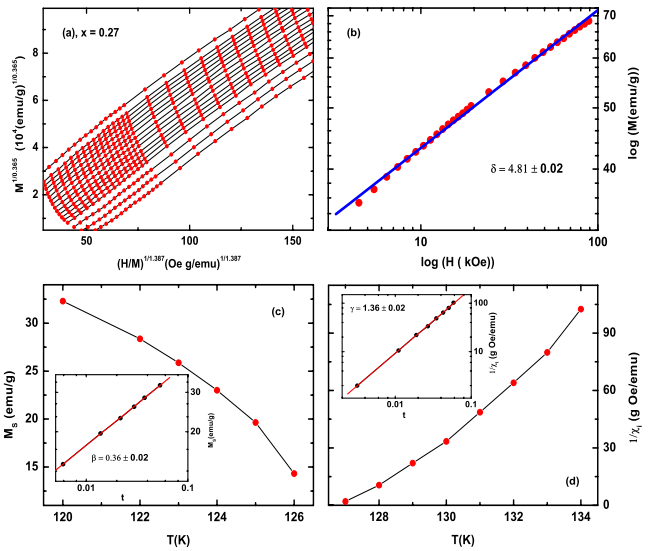

FIG. 5. (Color online) (a) Modified Arrot plots for $x=0.27$ using 3D-Heisenberg model exponents for a selection of magnetic isotherms from Fig. 1(b). (b) Double log plot of M vs H_i along critical isotherm, viz., $\log(M)$ vs $\log(H_i)$, $T_C=127$ K, yielding $\delta=4.78\pm0.03$ for 4 kOe$<H<$90 kOe. (c) The spontaneous magnetization $M_S(T)$ plotted against temperature: Inset; M_S vs reduced temperature t on a double-logarithmic scale, viz., $\log(M_S)$ vs $\log(t)$, the slope of the straight-line drawn yielding $\beta=0.36\pm0.02$. (d) The inverse initial susceptibility $1/\chi_i$ plotted against temperature: inset; $1/\chi_i$ vs reduced temperature t on a double-logarithmic scale, viz., $\log(1/\chi_i)$ vs $\log(t)$, the slope of the straight-line drawn yields $\gamma=1.36\pm0.02$.

The self-consistency of this determination is re-enforced in Figs. 5(b)–5(d) through the use of Eqs. (6)–(8). A double-logarithmic plot [Fig. 5(b)] of data along the critical isotherm $M(T_C=127\ \text{K},H)$ verifies the power-law prediction, and, for 4 kOe$<H<$90 kOe, yields the equation of state critical exponent $\delta=4.81\pm0.02$, which is again very close to the 3D-Heisenberg model prediction. The latter, incidentally, indicates—albeit indirectly—the absence of a Griffiths-type phase (GP) (frequently characterized by large δ values[31,33,39–41]) in the system; a point returned to below. Additionally, examination of the behavior of isotherms near T_C also reveals that they approach the expected shearing curve limited behavior:[28–30] the maximum slope of which yields a final estimate of the demagnetization factor $N_D=50\pm1$ g Oe/emu comparable with those given earlier.

The order-parameter exponent β can be derived from the spontaneous magnetization M_S [the abscissa in Fig. 5(a)] when plotted as a function of reduced temperature $t=(T-T_C)/T_C$; insert Fig. 5(c). Figure 5(d) displays the temperature dependence of the inverse initial susceptibility $1/\chi_i$ [the

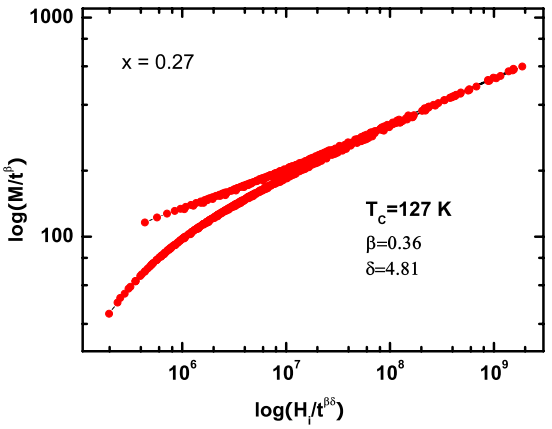

FIG. 6. (Color online) Conventional scaling plot for $x=0.27$ [Eq. (1)] on a double-logarithmic scale using the critical exponents and T_C listed above, viz., $\log(M/t^{\beta})$ vs $\log(H_i/t^{\beta\delta})$. The upper branch corresponds to data below T_C and the lower branch to data above T_C.

ordinates in Fig. 5(a)], replotted against reduced temperature in the corresponding insert. These inserts confirm the power-law predictions [Eqs. (6) and (7)], and the associated slopes yield exponents values of $\beta=0.36\pm0.02$ and $\gamma=1.36\pm0.02$, respectively. These estimates are again very close to Heisenberg model predictions.[35] A final assessment of scaling behavior both above and below $T_C=127$ K using the above-listed exponent estimates based on Eq. (1) is carried out in Fig. 6; the latter demonstrates good data collapse.

$x=0.29$

Figures 7(a)–7(e) summarize the corresponding analysis of the field-dependent ac susceptibility data at $x=0.29$ yielding $\delta=4.62\pm0.05$, $\gamma=1.38\pm0.01$, and $\beta=0.37\pm0.02$ with $T_C=114\pm0.5$ K. The first of these is slightly lower than Heisenberg model predictions, while the latter two are not. The field-dependent ac susceptibility data collapse, using these exponent values, is reproduced in Fig. 8. The magnetization data for this sample are, however, slightly more complex. Figure 9(a) demonstrates that modified Arrott plots using near-Heisenberg model exponents exhibit slight curvature unlike the situation encountered at $x=0.27$. Nevertheless, with $T_C=114\pm0.5$ K found from extrapolating low-field data in Fig. 9(a), not only is the equation of state exponent (deduced over a comparable field range along the critical isotherm to that utilized at the lower composition) consistent with that found from the ac susceptibility analysis, viz., $\delta=4.6\pm0.1$ [Fig. 9(b)], but scaling of the magnetization data over a comparable range of field and reduced temperature is also achieved [Fig. 9(c)] with the same value for $\delta=4.6$ and $\beta=0.36$.

Both the curvature and the (slightly) depressed δ value mentioned above are qualitatively consistent with the increasing presence of AFM interactions as x increases. The presence of the latter constitutes disorder—specifically disorder in the exchange bond distribution—which, by broadening the (assumed) Gaussian exchange bond distribution, can lead to reduced values for the effective exponent δ^*.[17] It

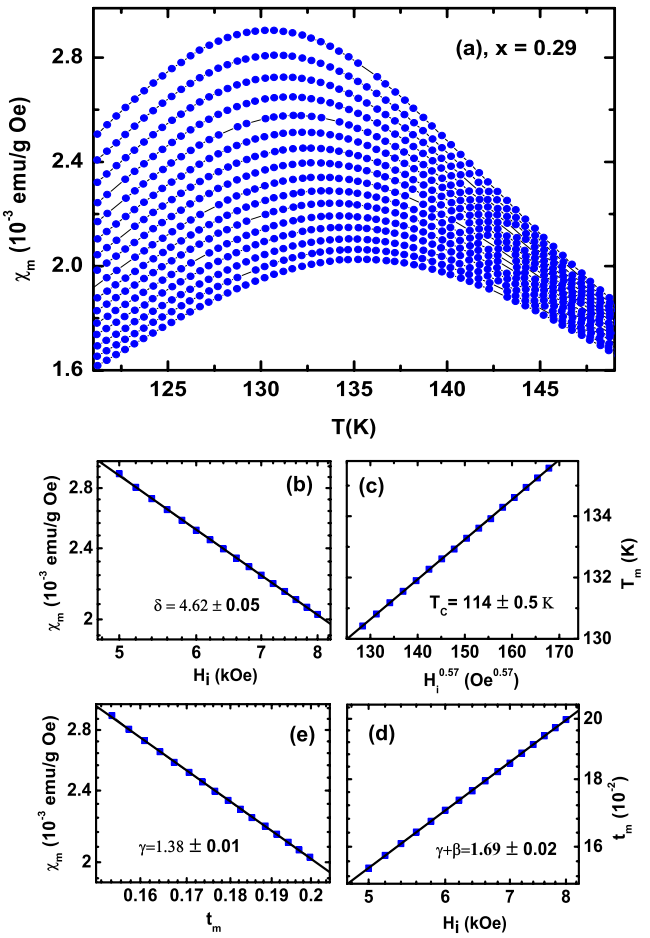

FIG. 7. (Color online) (a) $\chi(H,T)$ for $x=0.29$ (corrected for background and demagnetizing effects) measured on warming following ZFC in fixed static fields of 5 kOe (top) to 8 kOe (bottom) in 200 Oe steps. (b) Double-logarithmic plot testing the power-law prediction of Eq. (3), viz., $\log(\chi_m)$ vs $\log(H_i)$, the slope yielding $\delta=4.62\pm0.05$. (c) Estimate of critical temperature $T_C=114\pm0.5$ K from extrapolation of the susceptibility peak temperatures (T_m) against ($H_i^{0.57}$). Double-logarithmic plots testing the remaining power-law predictions [Eqs. (4) and (5)]. (d) The reduced peak temperature (t_m) against the internal field (H_i), viz., $\log(t_m)$ vs $\log(H_i)$, yielding $\gamma+\beta=1.69\pm0.02$. (e) The peak susceptibilities (χ_m) against reduced temperature (t_m), viz., $\log(\chi_m)$ vs $\log(t_m)$, yielding $\gamma=1.37\pm0.02$ and hence $\beta=0.36\pm0.02$.

should also be conceded that the composition of this sample places it close to the boundary for charge ordering; the precursor effects of which *may* play some role in this context, although such effects have yet to be addressed in any detail experimentally or theoretically. The disorder discussed above is not, however, effective in nucleating a GP-type feature in either specimen. The "normal"—as opposed to substantially enhanced—δ values indirectly support this assertion as mentioned earlier, while the temperature dependence of the inverse (zero-field) susceptibility [shown in the insert in Fig. 2(a) for $x=0.27$] confirms it directly by not displaying the downturn characteristic of large cluster/correlated volume formation within such a phase [GP characteristics can display a marked sensitivity to applied field,[31,33,39,40] thus the use of the zero-field response (i.e., using only in an ac driv-

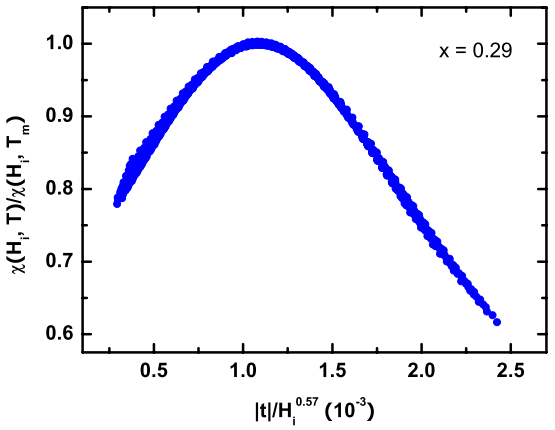

FIG. 8. (Color online) Scaling plot for the isokaps in Fig. 7(a) for $x=0.29$.

ing field of 1 Oe rms) provides the more appropriate measure[41]]. Another feature linked with the occurrence of a GP has been an anomalous variation in the behavior of the acoustic spin-wave stiffness D.[33,42] To investigate the latter in the present samples, measurements of the magnetization that have been carried out in 2 K steps up to approximately half the ordering temperature $(T_C/2)$ and estimates made of the spontaneous magnetization $[M_S(T)]$ using extrapolations based on a modified Arrott-Noakes equation of state.[22,23] These estimates are reproduced in Fig. 10(a) from which the following conclusions can be drawn. First, the spontaneous magnetization $[M_S(T)]$ at zero temperature is estimated to be $M_S(0)=91.9\pm0.2$ emu/g$=3.57\pm0.02$ μ_B at $x=0.27$ and $M_S(0)=88.2\pm0.2$ emu/g$=3.39\pm0.02$ μ_B at $x=0.29$: both of which are smaller than the respective theoretical spin-only moment values of $M_S(0)=3.73$ and 3.71 μ_B. The latter indicates a small degree of noncollinearity in moments—possibly the Pr moment—in both samples.[10] In the absence of detailed microscopic measurements, however, a rough estimate of the average degree of noncollinearity can be found using $\theta=\cos^{-1}[M_S(0)/M_{\rm sat}]=17°$ and 24°, respectively, for $x=0.27$ and 0.29.[43] Second, these data have been fit to the Bloch $T^{3/2}$ law;[44,45] such a temperature dependence originates from the assumption of gapless acoustic spin-wave excitations described in the usual notation by the dispersion relation $\hbar\omega_{\rm ac}=Dq^2$ and leads to the following well-known expression for the temperature dependence of $M_S(T)$,[25,44,45] viz.:

$$\frac{M_s(T)}{M_S(0)} = 1 - \frac{1}{NS}\left(\frac{k_BT}{4\pi D(T)}\right)^{3/2}\xi\left(\frac{3}{2}\right). \qquad (9)$$

Here $\xi(3/2)$ is the Riemann zeta function and D the acoustic spin-wave stiffness. A least-square fitting of Eq. (9) to the data yield $D(0)=70\pm1$ meV Å^2 $(x=0.27)$ and $D(0)=75\pm2$ meV Å^2 $(x=0.29)$ values close to that estimated from neutron-scattering data on a $Pr_{0.75}Ca_{0.25}MnO_3$ single crystal $[D(0)=60$ meV Å$^2]$.[14] As reported previously, these latter values for D are comparable to those found in the ground state of other FM insulating manganites, such as $La_{0.8}Ca_{0.2}MnO_3$,[33,42] and indeed in the ZFC charge-ordered insulating ground state of this same system.[46] In contrast, in

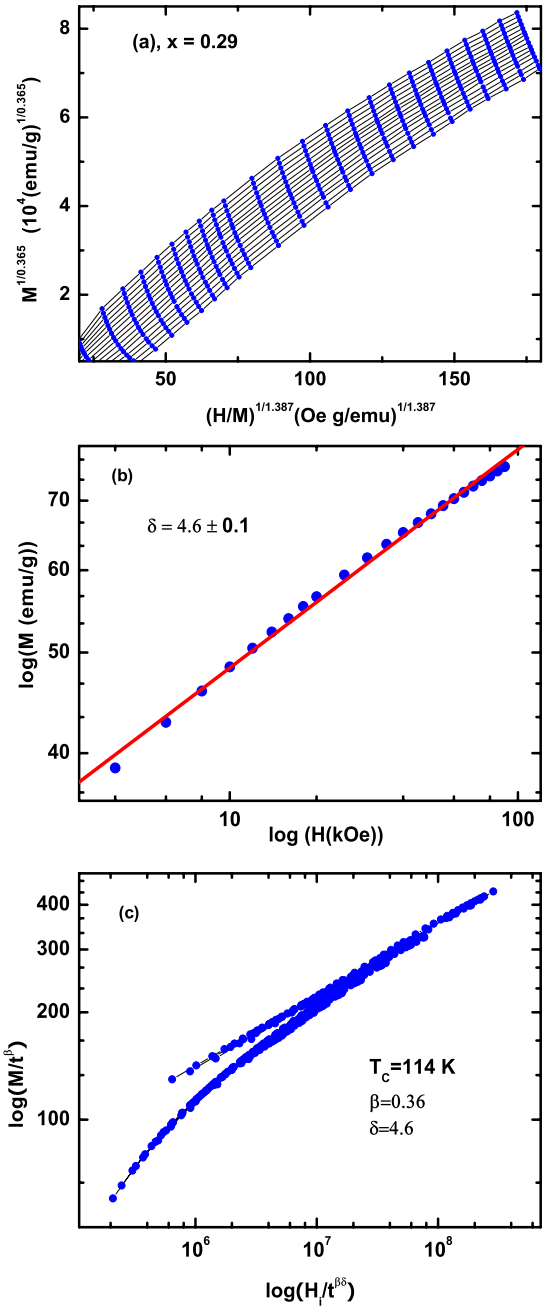

FIG. 9. (Color online) (a) Modified Arrot plots for $x=0.29$ using 3D-Heisenberg model exponents in the temperatures of 110 K to 125 K in 1 K steps. (b) The critical isotherm $T_C=114$ K replotted on double-logarithmic scale, viz., $\log(M)$ vs $\log(H_i)$, estimation from the data 4 kOe$<H<$90 kOe incorporating Eq. (8) yielding a value of $\delta=4.6\pm0.1$. (c) Conventional scaling plot—Eq. (1)—replotted on a double-logarithmic scale $[\log(M/t^\beta)$ vs $\log(H_i/t^{\beta\delta})]$ using the critical exponents and T_C listed above.

the field-induced FM metallic state of this system, D is enhanced by close to a factor of 3 reaching values approaching 150 meV Å^2 in both single crystal $Pr_{0.7}Ca_{0.3}MnO_3$ (Ref. 47) and polycrystalline $Pr_{0.6}Ca_{0.4}MnO_3$.[46] This marked change in D with composition and field summarized in Fig. 10(b) demonstrates that D can monitor the occurrence of charge order-

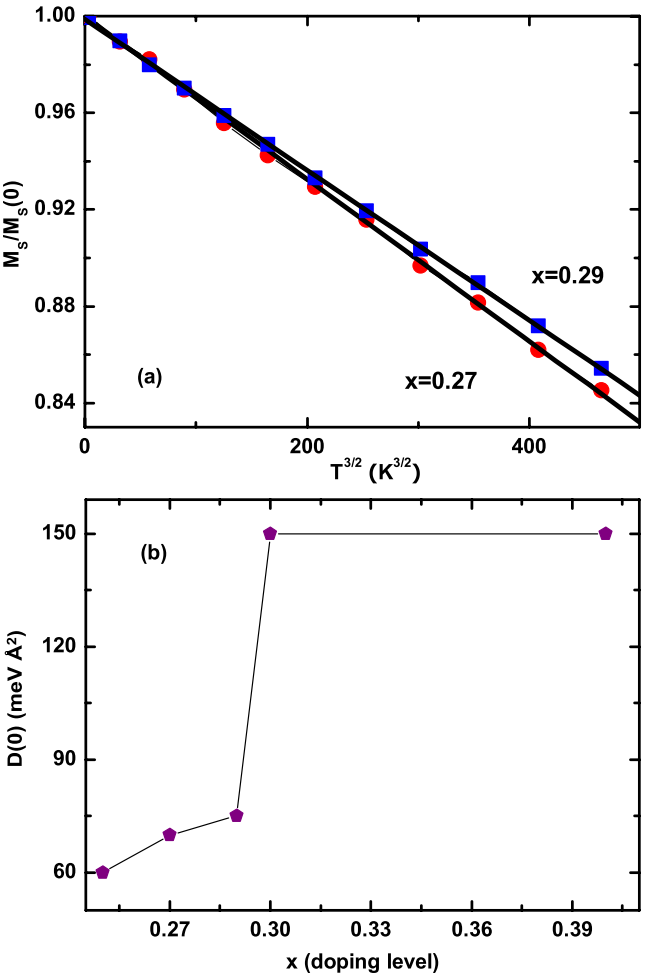

FIG. 10. (Color online) (a) The low-temperature-reduced spontaneous magnetization $M_S(T)/M_S(0)$ plotted against $T^{3/2}$. (b) The evolution of the acoustic spin-wave stiffness of $D(0)$ as a function of doping level (x) in $Pr_{1-x}Ca_xMnO_3$ compounds.

ing in a comparably striking manner to that shown by recent studies of the EFG in this system.[19]

IV. TRANSPORT PROPERTIES

For completeness, the transport behavior of these samples was also investigated. In the strictest sense of charge ordering, no hopping contribution to the conductivity would occur; at least in the conventional DE scenario where uncorrelated hopping via a single intermediate oxygen atom alone is considered. The present specimens lie outside such a regime. Figures 11(a) and 11(b) [(x=0.27) and (x=0.29)] confirm that below the charge-ordered regime ($x>0.3$) of this system, available fields are unable to melt the FM insulating ground state;[9,10] conversely the retention of insulating characteristics in high-applied fields provided indirect evidence against the occurrence of charge ordering. The continuous semiconductorlike increase in the samples resistance with decreasing temperature precluded measurements being carried out below 90 K. Nevertheless, the emergence of a small cusp near $T=125$ K (x=0.27), the previously determined ordering temperature for $H=0$ indicates that magnetic ordering influences the conduction process (albeit not nearly as dramatically as in "conventional" DE systems); an assertion confirmed by the associated magnetoresistance [insert in

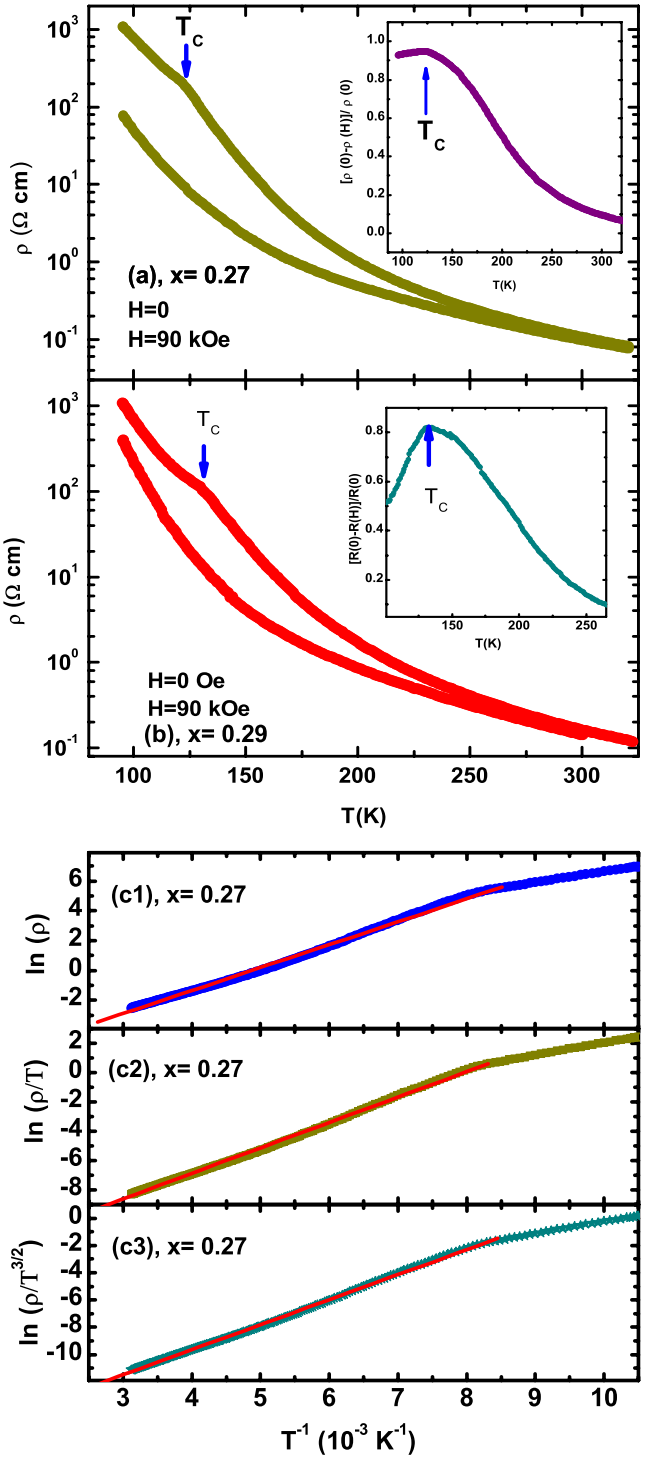

FIG. 11. (Color online) (a) Resistivity for x=0.27 in zero field (top); 90 kOe (bottom) measured on warming following ZFC: Insert is the magnetoresistance $[\rho(0)-\rho(H)]/\rho(0)$ exhibiting a peak at T_C. (b) as in (a) for x=0.29. (c) Data (x=0.27) fits to the linearized forms of Eq. (10) for simple thermal excitation (c1), adiabatic SPH model (c2), and nondiabatic SPH model (c3).

Figs. 11(a) and 11(b)]. The behavior of the resistivity in the PM insulating phase ($d\rho/dT<0$) above T_C in many doped Mn perovskites has been fitted to a modified Arrhenius law of the form[48–50]

$$\rho(T) = \rho_0 T^{\alpha} \exp(E_a/k_B T), \tag{10}$$

where E_a is an activation energy while the exponent α can assume values of 0, 1, or 3/2 depending on the physical model invoked [i.e., zero for simple thermally activated hopping, one for adiabatic, and 3/2 for nonadiabatic small polaron hopping (SPH) (Refs. 48–50)]. The prefactor ρ_0 includes a factor $x(1-x)$ (x being the doping level) to account for site-occupation effects.[48,49] For the present single crystals, the nonadiabatic SPH model ($\alpha=3/2$) provides the most convincing fit to available data in the high-temperature regime. Such fits shown in Fig. 11(c) using the linearized form of Eq. (10) yield $E_a=155.4$ meV for the zero-field data at $x=0.27$, which is very close to the corresponding estimate of $E_a=158.1$ meV at $x=0.29$ (and hence not reproduced here). These estimates for E_a agree with the overall range of those obtained from zero-field data on a range of manganites.[48,49]

V. SUMMARY AND CONCLUSIONS

Detailed analysis of field- and temperature-dependent ac susceptibility and magnetization data in single crystal $Pr_{1-x}Ca_xMnO_3$ ($x=0.27$, and 0.29) reveals near-Heisenberg model exponents, so that the lack of metallicity and the suppression of charge fluctuations in them do not appear to influence the universality class of the FM-PM transition. Indeed, these exponent values agree with the predictions for the universality class of the DE model in the absence of significant anisotropy effects.[51,52] Specifically for $x=0.27$, $\delta=4.81\pm0.02$, $\gamma=1.36\pm0.02$, and $\beta=0.36\pm0.02$ (consistent with the predictions for the nearest-neighbor 3D Heisenberg model) with $T_C=127\pm0.5$ K; whereas at $x=0.29$ the exponents are marginally different, with $\delta=4.62\pm0.05$, $\gamma=1.38\pm0.01$, $\beta=0.37\pm0.02$, and $T_C=114\pm0.5$ K. Qualitatively, these small changes likely reflect the rising importance of AFM interactions with increasing x as the charge-ordered state is approached: an influence that is difficult to assess quantitatively. No evidence for a GP was found in either specimen. These single crystals also display comparable values of the acoustic spin-wave stiffness $D\sim70$ meV Å^2, well below that found in the charge-ordered field-induced metallic regime of the same system. These samples remain insulators below FM ordering temperature T_C in fields up to 90 kOe; they display nonabiabatic SPH-mediated transport behavior in the PM regime in zero field characterized by activation energies comparable to those reported for a range of doped perovskites.

ACKNOWLEDGMENTS

Support for this work by the Natural Sciences and Engineering Research Council (NSERC) of Canada and the University of Manitoba (W.J.) are gratefully acknowledged.

*jiang@physics.umanitoba.ca

[1] J. Orenstein and A. J. Millis, Science **288**, 468 (2000).
[2] C. Zener, Phys. Rev. **81**, 440 (1951); S. Wang and C. W. Searle, Can. J. Phys. **49**, 387 (1970).
[3] A. Moreo, S. Yunoki, and E. Dagotto, Science **283**, 2034 (1999); E. Dagotto, *Phase Separation and Colossal Magnetoresistance* (Springer, Berlin, 2002); E. Dagotto, Science **309**, 257 (2005).
[4] *Colossal Magneto-resistive Oxides*, edited by Y. Tokura (Gordon and Breach, New York, 2000); Y. Tokura and N. Nagaosa, Science **288**, 462 (2000).
[5] J. M. D. Coey, M. Viret, and S. V. Molnar, Adv. Phys. **48**, 167 (1999).
[6] W. Eerenstein, N. D. Mathur, and J. F. Scott, Nature (London) **442**, 759 (2006).
[7] Seongsu Lee, A. Pirogov, Misun Kang, Kwang-Hyun Jang, M. Yonemura, T. Kamiyama, S.-W. Cheong, F. Gozzo, Namsoo Shin, H. Kimura, Y. Noda, and J.-G. Park, Nature (London) **451**, 805 (2008).
[8] J. B. Goodenough, Rep. Prog. Phys. **67**, 1915 (2004); L. M. Rodriguez-Martinez and J. P. Attfield, Phys. Rev. B **54**, R15622 (1996).
[9] Y. Tomioka, A. Asamitsu, H. Kuwahara, Y. Moritomo, and Y. Tokura, Phys. Rev. B **53**, R1689 (1996).
[10] H. Yoshizawa, H. Kawano, Y. Tomioka, and Y. Tokura, Phys. Rev. B **52**, R13145 (1995).
[11] V. Kiryukhin, D. Casa, J. P. Hill, B. Keimer, A. Vigliante, Y. Tomioka, and Y. Tokura, Nature (London) **386**, 813 (1997).
[12] A. Asamitsu, Y. Tomioka, H. Kuwahara, and Y. Tokura, Nature (London) **388**, 50 (1997).
[13] K. Miyano, T. Tanaka, Y. Tomioka, and Y. Tokura, Phys. Rev. Lett. **78**, 4257 (1997).
[14] R. Kajimoto, H. Mochizuki, H. Yoshizawa, S. Okamoto, and S. Ishihara, Phys. Rev. B **69**, 054433 (2004).
[15] P. W. Anderson, Phys. Rev. **79**, 350 (1950).
[16] D. Sherrington and S. Kirkpatrick, Phys. Rev. Lett. **35**, 1792 (1975); K. Binder and A. P. Young, Rev. Mod. Phys. **58**, 801 (1986).
[17] A. Peles, H. P. Kunkel, X. Z. Zhou, and Gwyn Williams, J. Phys.: Condens. Matter **11**, 8111 (1999); Gwyn Williams, in *Magnetic Susceptibility of Superconductors and Other Spin Systems*, edited by R. A. Hein *et al.* (Plenum, New York, 1991), p. 475; X. Z. Zhou, H. P. Kunkel, J. H. Zhao, P. A. Stampe, and Gwyn Williams, Phys. Rev. B **56**, R12714 (1997); R. M. Roshko and Gwyn Williams, J. Phys. F: Met. Phys. **14**, 703 (1984); K. Kornik, H. P. Kunkel, R. M. Roshko, and Gwyn Williams, Solid State Commun. **76**, 993 (1990).
[18] B. W. Southern, J. Phys. C **9**, 4011 (1976); T. Kaneyoshi, *ibid.* **8**, 3415 (1975); C. Loewen and R. M. Roshko, Phys. Rev. B **31**, 4663 (1985).
[19] A. M. L. Lopes, J. P. Araújo, V. S. Amaral, J. G. Correia, Y. Tomioka, and Y. Tokura, Phys. Rev. Lett. **100**, 155702 (2008).
[20] L. M. Fisher, A. V. Kalinov, I. F. Voloshin, N. A. Babushkina, K.

I. Kugel, and D. I. Khomskii, Phys. Rev. B **68**, 174403 (2003).
[21] D. Shulyatev, S. Karabashev, A. Arsenov, and Y. Mukovskii, J. Cryst. Growth **198-199**, 511 (1999).
[22] A. Arrott and J. E. Noakes, Phys. Rev. Lett. **19**, 786 (1967).
[23] A. Arrott, Phys. Rev. **108**, 1394 (1957).
[24] Wei Li, H. P. Kunkel, X. Z. Zhou, Gwyn Williams, Y. Mukovskii, and D. Shulyatev, J. Phys.: Condens. Matter **16**, L109 (2004).
[25] T. Brown, Wei Li, H. P. Kunkel, X. Z. Zhou, Gwyn Williams, Y. Mukovskii, and A. Arsenov, J. Phys.: Condens. Matter **17**, 5997 (2005).
[26] I. G. Deac, J. F. Mitchell, and P. Schiffer, Phys. Rev. B **63**, 172408 (2001).
[27] T. Song, R. M. Roshko, and E. D. Dahlberg, J. Phys.: Condens. Matter **13**, 3443 (2001); G. Bertotti, *Hysteresis in Magnetism* (Academic, New York, 1998).
[28] Gwyn Williams, J. Alloys Compd. **326**, 36 (2001).
[29] J. H. Zhao, H. P. Kunkel, X. Z. Zhou, Gwyn Williams, and M. A. Subramanian, Phys. Rev. Lett. **83**, 219 (1999).
[30] Wei Li, H. P. Kunkel, X. Z. Zhou, Gwyn Williams, Y. Mukovskii, and D. Shulyatev, Phys. Rev. B **70**, 214413 (2004).
[31] Wanjun Jiang, X. Z. Zhou, Gwyn Williams, Y. Mukovskii, and K. Glazyrin, Phys. Rev. B **77**, 064424 (2008).
[32] Wei Li, H. P. Kunkel, X. Z. Zhou, Gwyn Williams, Y. Mukovskii, and D. Shulyatev, Phys. Rev. B **75**, 012406 (2007).
[33] Wanjun Jiang, X. Z. Zhou, Gwyn Williams, Y. Mukovskii, and K. Glazyrin, Phys. Rev. Lett. **99**, 177203 (2007).
[34] H. E. Stanley, *Introduction to Phase Transitions and Critical Phenomena* (Clarendon, Oxford, 1971).
[35] M. Campostrini, M. Hasenbusch, A. Pelissetto, P. Rossi, and E. Vicari, Phys. Rev. B **65**, 144520 (2002).
[36] Z. Wang, H. P. Kunkel, and Gwyn Williams, J. Phys.: Condens. Matter **4**, 10385 (1992).
[37] K. Ghosh, C. J. Lobb, R. L. Greene, S. G. Karabashev, D. A. Shulyatev, A. A. Arsenov, and Y. Mukovskii, Phys. Rev. Lett. **81**, 4740 (1998); D. Kim, B. L. Zink, F. Hellman, and J. M. D. Coey, Phys. Rev. B **65**, 214424 (2002).
[38] D. Kim, B. Revaz, B. L. Zink, F. Hellman, J. J. Rhyne, and J. F. Mitchell, Phys. Rev. Lett. **89**, 227202 (2002).
[39] Wanjun Jiang, X. Z. Zhou, Gwyn Williams, Y. Mukovskii, and K. Glazyrin, Phys. Rev. B **76**, 092404 (2007).
[40] M. B. Salamon, P. Lin, and S. H. Chun, Phys. Rev. Lett. **88**, 197203 (2002).
[41] Wanjun Jiang, X. Z. Zhou, and Gwyn Williams, arXiv:0806.1003 (unpublished).
[42] T. Okuda, Y. Tomioka, A. Asamitsu, and Y. Tokura, Phys. Rev. B **61**, 8009 (2000).
[43] P.-G. de Gennes, Phys. Rev. **118**, 141 (1960).
[44] F. Keffer, *Spin Waves (Handbuch der Physik)* (Springer, Berlin, 1966), Vol. VIII/2.
[45] C. Kittel, *Introduction to Solid State Physics*, 2nd ed. (Wiley, New York, 1976).
[46] G. X. Cao, J. C. Zhang, B. J. Kang, Y. N. Sha, S. X. Cao, and X. C. Shen, Europhys. Lett. **81**, 17003 (2008).
[47] F. Ye, P. C. Dai, J. A. Fernandez-Baca, Hao Sha, J. W. Lynn, H. Kawano-Furukawa, Y. Tomioka, Y. Tokura, and J. D. Zhang, Phys. Rev. Lett. **96**, 047204 (2006); Hao Sha, F. Ye, P. Dai, J. A. Fernandez-Baca, D. Mesa, J. W. Lynn, Y. Tomioka, Y. Tokura, and J. D. Zhang, Phys. Rev. B **78**, 052410 (2008).
[48] D. C. Worledge, L. Miéville, and T. H. Geballe, Phys. Rev. B **57**, 15267 (1998).
[49] M. Ziese and C. Srinitiwarawong, Phys. Rev. B **58**, 11519 (1998).
[50] B. I. Shklovskii and A. L. Efros, *Electronic Properties of Doped Semiconductors*, Springer Series in Solid-State Sciences (Springer, New York, 1984).
[51] J. L. Alonso, L. A. Fernández, F. Guinea, V. Laliena, and V. Martín-Mayor, Nucl. Phys. B **596**, 587 (2001).
[52] Y. Motome and N. Furukawa, J. Phys. Soc. Jpn. **68**, 3853 (1999); **69**, 3785 (2000); **70**, 1487 (2001).